Non-linear hybrid kinetic-MHD simulations of ELMs in the ASDEX Upgrade tokamak

J. Dominguez-Palacios[1,2], J. Gonzalez-Martin[2,3], M. Garcia-Munoz[1,2],
M. Toscano-Jimenez[4], E. Viezzer[1,2], S. Futatani[5], J. Galdon-Quiroga[6], M. Hoelzl[6],
P. Oyola[1], J. Rivero-Rodriguez[2,3], C. Soria-Hoyo[7], Y. Suzuki[8], Y. Todo[8],
the ASDEX Upgrade[6,i] and EUROfusion MST1[ii] Teams

[1] *Department of Atomic, Nuclear and Molecular Physics, University of Seville, Spain*

[2] *CNA, Universidad de Sevilla, CSIC, Junta de Andalucía*

[3] *Department of Mechanical Engineering and Manufacturing, University of Seville, Spain*

[4] *Department of Applied Physics III, University of Seville, Spain*

[5] *Universitat Politècnica de Catalunya, Barcelona, Spain*

[6] *Max-Planck-Institut für Plasmaphysik, Garching, Germany*

[7] *Department of Electronics and Electromagnetism, University of Seville, Spain*

[8] *National Institute for Fusion Science, Toki, Japan*

Introduction

Edge localized modes (ELMs) [1, 2] are quasiperiodic magnetohydrodynamic (MHD) instabilities that routinely appear in H-mode plasmas, driven by large edge pressure gradients and current densities. They expel particles and heat towards the first wall, which reduces the lifetime of plasma-facing components and could limit the performance of future fusion devices [3]. Thus, a detailed understanding of edge stability and ELM control is needed.

Recent experimental observations have revealed that ELMs can interact with fast-ion population. Fast-ion loss detector (FILD) measurements have shown fast-ion losses [4] and acceleration during ELMs [5]. These results manifest the need for a kinetic description of fast-ions in ELM modelling. In this sense, the non-linear hybrid kinetic-MHD MEGA code [6, 7] may help to disentangle the physical mechanisms behind the interplay between fast-ions and ELMs.

In this work, we adapt the MHD module of MEGA, MIPS [8], to resolve edge instabilities and apply it to ASDEX Upgrade (AUG) discharge #33616 [9]. Edge ballooning structures are identified in these simulations. Furthermore, the impact of diamagnetic, toroidal and recently implemented neoclassical flows on ELM stability is addressed.

---

[i] See author list of H. Meyer *et al*., Nucl. Fusion accepted (2019).
[ii] See author list of B. Labit *et al*., Nucl. Fusion **59** 086020 (2019).

Simulation model and inputs

The bulk plasma is described by the non-linear MHD equations in the MIPS code, using standard MHD [10] or extended MHD [11], which includes diamagnetic and toroidal flows. To consider neoclassical flows in the extended MHD model, we add to the right-hand side of the momentum equation the divergence of the neoclassical stress tensor [12],

$$-\nabla \cdot \overline{\overline{\Pi}}_{\mathrm{neo}} = -\rho \mu_{\mathrm{neo}} \frac{B^2}{B_\theta^2} \left(v_\theta + v_{\mathrm{pi},\theta} - v_{\theta,\mathrm{neo}}\right) \hat{e}_\theta, \quad (1)$$

where ρ, μ_{neo}, B_θ, v_θ, $v_{\mathrm{pi},\theta}$ and $\hat{e}_\theta$ are the mass density, neoclassical friction coefficient, poloidal magnetic field, poloidal velocity, poloidal diamagnetic flow and unit vector in the poloidal direction of the magnetic field, respectively. Equation (1) accounts for the friction between trapped and passing thermal ions, which is important at the pedestal due to the steep gradients. This expression constrains the total poloidal velocity to approach the value predicted by neoclassical theory $v_{\theta,\mathrm{neo}} = -k\, \nabla T \times B/2eB^2 \cdot \hat{e}_\theta$, where k is the neoclassical heat diffusivity. It is assumed $k = -1$ and $\mu_{\mathrm{neo}} = 10^{-6}\omega_{\mathrm{D}}$, with $\omega_{\mathrm{D}} = 1.18 \times 10^8$ s^{-1} being the deuterium gyrofrequency at the magnetic axis. The resistivity η, the viscosity ν, the particle diffusivity D and the parallel and perpendicular heat diffusivities $\chi_\parallel$ and $\chi_\perp$ are used and take the values $\eta/\mu_0 = D = 10^{-6} v_{\mathrm{A}} R_0$, $\nu = 10^{-5} v_{\mathrm{A}} R_0$, $\chi_\perp = 5 \times 10^{-7} v_{\mathrm{A}} R_0$ and $\chi_\parallel = 10^5 \chi_\perp$, where $v_{\mathrm{A}} = 4.40 \times 10^6$ ms^{-1} and $R_0 = 1.64$ m denote the Alfvén velocity at the magnetic axis and the major radius, respectively.

The initial conditions used are a pre-ELM equilibrium reconstruction of AUG shot #33616 at 7.2 s based on kinetic profiles just before the ELM crash averaged over several ELM cycles, using the CLISTE code [13]. Experimentally, the ELM crash is dominated by n~2-5 modes [9]. Non-linear MHD JOREK simulations agree with these findings [14]. Kinetic and rotation profiles as a function of normalized poloidal flux ρ_{pol} used hereafter are shown in figure 1. The equations are

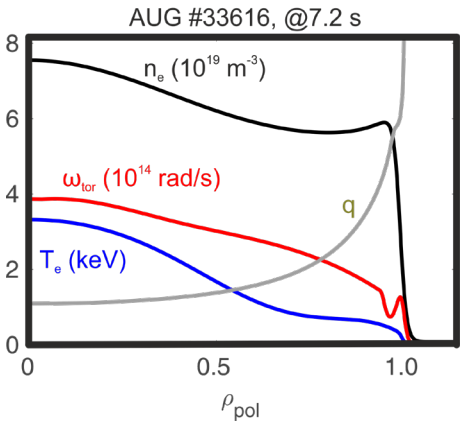

Figure 1: Electron density (n_e), electron temperature (T_e), toroidal rotation (ω_{tor}) and safety factor (q) profiles.

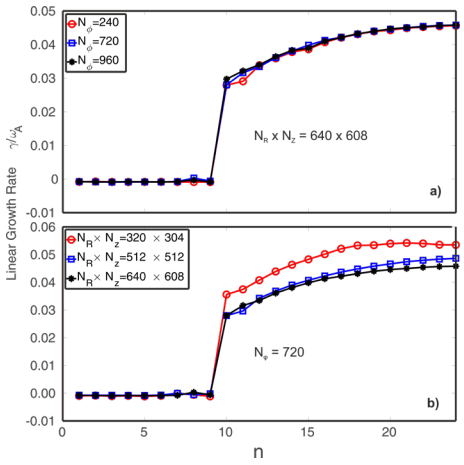

Figure 2: Linear growth rates normalized by $\omega_A = v_A/R_0$ in standard MHD, for fixed poloidal mesh (a) and fixed toroidal mesh (b).

solved in the rectangular grids of cylindrical coordinates (R, φ, z) with (512, 720, 512) grid points. The simulation domain includes the scrape-off layer (SOL) and the private flux region, both modelled as a low-density plasma ($n_e \sim 7.5 \times 10^{-17} \mathrm{m}^{-3}$). MIPS filters out toroidal Fourier modes above $n > 24$ to reduce the numerical noise. Spatial derivatives are evaluated using a fourth-order finite difference scheme and the time evolution is calculated using a fourth-order explicit Runge-Kutta method. An initial weak perturbation is applied in $0.9 < \rho_{\mathrm{pol}} < 1.05$ to allow the modes to start growing. Flows are neglected in $\rho_{\mathrm{pol}} > 1.03$, and the magnetic field is constant at the boundary of the simulation domain.

Simulation results

A: Ballooning modes in standard MHD simulations

In our MIPS simulations, edge ballooning modes can be identified. A numerical convergence test has been performed to ensure the grid resolution does not affect our results (see figure 2). Figure 3 shows the time evolution of the magnetic energy of each toroidal mode using standard MHD. In the linear phase, high n harmonics (n~20) are the most unstable. Figure 4a) reveals that the perturbation is located at the Low Field Side (LFS). Moreover, figure 4b) illustrates the radial profile of n = 22, showing several poloidal harmonics located at the pedestal. Therefore, these instabilities are ballooning modes. At $t/\tau_A \approx 32$, quadratic mode coupling enhances the growth of lower n modes (n~1-9) [15]. During the non-linear phase, heat and particle transport is triggered. Figure 5 depicts the time evolution of the thermal energy and the number of thermal particles. As lower n modes start growing due to non-linear coupling, the thermal energy and number of particles decrease inside the separatrix and increase outside it, which indicates a transport of these quantities towards the SOL.

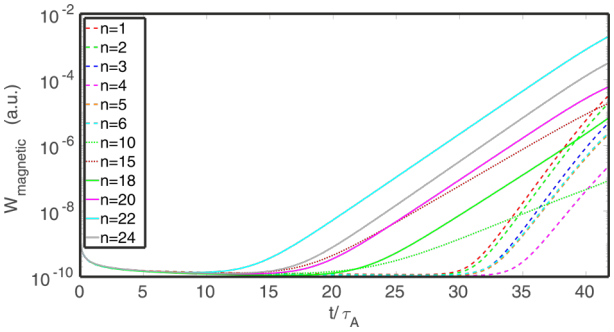

Figure 3: Time evolution of magnetic energy contained in the harmonics using standard MHD.

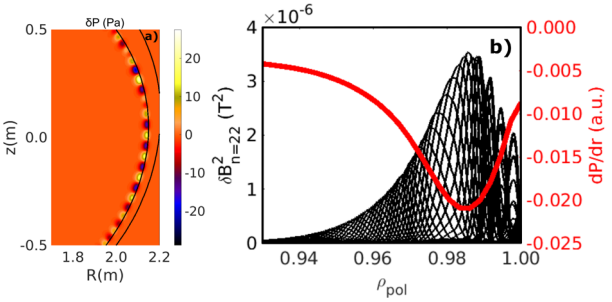

Figure 4: (a) Pressure perturbation in the poloidal plane at the LFS, t = 27 τ_A. (b) Smoothed radial profiles of the poloidal harmonics of n = 22 (black) and equilibrium pressure gradient (red).

B: Mode stability in extended MHD

Extended MHD simulations are carried out, as diamagnetic, toroidal and neoclassical

flows may have an impact on ELM stability. Figure 6 shows the linear growth rates of the harmonics considered in standard and extended MHD. The growth rate of high n modes decreases when diamagnetic and toroidal flows are included. Neoclassical flows hardly alter their growth in our simulations. This could be solved by increasing the value of μ_{neo}.

Conclusions and outlook

The MIPS code has been extended to simulate edge instabilities. Edge ballooning modes have been observed in the simulations. Diamagnetic and toroidal flows diminish high n harmonic growth rates obtained in standard MHD, although they are not linearly stable. The results obtained here still differ from what is experimentally observed [9] and from what JOREK simulations predict [14]. At this stage, a direct comparison between our results and those found in Ref. [14] is not possible, since the physics and parameters considered in this work differ from JOREK. Obtaining a linear phase dominate by lower n modes is, therefore, the subject of our future work. A scan varying μ_{neo} will be performed to see the impact of neoclassical flows on ELM stability.

Acknowledgements

This work has been carried out within the framework of the EUROfusion Consortium and has received funding from the Euratom research and training programme 2014-2018 and 2019- 2020 under Grant Agreement No. 633053. The views and opinions expressed herein do not necessarily reflect those of the European Commission. The author thankfully acknowledges the support from Marconi, for its provision of computing resources under the scope of project MEGAEDGE, and the computer resources at MareNostrum and the technical support provided by Barcelona Supercomputing Centre (RES-FI-2019-1-0034).

References

[1] H. Zohm, Plasma Phys. Control. Fusion **38**, 105 (1996).
[2] E. Viezzer *et al.*, Invited Talk I4.101, this conference.
[3] R.P. Wenninger *et al.*, Nucl. Fusion **54**, 114003 (2014).
[4] M. Garcia-Munoz *et al.*, Nucl. Fusion **53**, 123008 (2013).
[5] J. Galdon-Quiroga *et al.*, Phys. Rev. Lett. **121**, 025002 (2018).
[6] Y. Todo *et al.*, Phys. Plasmas **5**, 1321 (1998).
[7] Y. Todo *et al.*, Invited Talk I1.104, this conference.
[8] Y. Todo *et al.*, Plasma and Fusion Res. **5**, S2062 (2010).
[9] A. F. Mink *et al.*, Nucl. Fusion **58**, 026011 (2018).
[10] Y. Todo *et al.*, Phys. Plasmas **24**, 081203 (2017).
[11] Y. Todo *et al.*, Nucl. Fusion **56**, 112008 (2016).
[12] F. Orain *et al.*, Phys. Plasmas **20**, 102510 (2013).
[13] P.J. McCarthy, Phys. Plasmas **6**, 3554 (1999).
[14] M. Hoelzl *et al.*, Contrib. Plasma Phys. **58**, 518-28 (2018).
[15] I. Krebs *et al.*, Phys. Plasmas **20**, 082506 (2013).

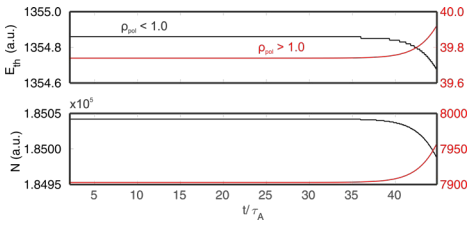

Figure 5: Time evolution of thermal energy and number of particles inside (black) and outside (red) the separatrix.

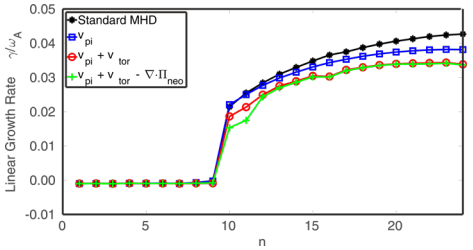

Figure 6: Linear growth rates using standard and extended MHD.